Phase Stability and Morphology of Gel Grown Crystals: The Case of CdCl$_2$-bpp Polymeric System

Leonardo Lo Presti [1,2,3], **Massimo Moret** [4] **and Silvia Rizzato** [1,*]

[1] Dipartimento di Chimica, Università degli Studi di Milano, via Golgi 19, I-20133 Milano, Italy
[2] ISTM-CNR, Via Golgi 19, 20133 Milano, Italy
[3] Centre for Materials Crystallography, Aarhus University, Langelandsgade 140, DK-8000 Aarhus, Denmark
[4] Dipartimento di Scienza dei Materiali, Università degli Studi di Milano Bicocca, via Cozzi 55, I-20125 Milano, Italy
[*] Correspondence: silvia.rizzato@unimi.it

Abstract: A phenomenological study is carried out on a complex two-component diffusion-reacting system in gel, that is, the Cd-*1,3-bis(4-pyridyl)propane* (Cd-bpp) coordination polymer. The latter can exist in three solid forms, which exploit a 1:1 correspondence among the Cd/bpp ratio, the crystal structure and the crystal morphology (1/2: bipyramids; 2/3: needles; 1/3: plates). The aim was to clarify the role of key physicochemical variables (reactant concentrations, composition of the solvent and density of the transport medium) in determining the chemical nature and the morphology of the final crystallization products. The gel method was tested in a variety of different crystallization configurations, including single and double diffusion techniques. The density of the gel primarily affects the morphology of the synthesized crystals, with denser media favouring the needle-like 2/3 Cd-bpp species and diluted ones the 1/2 Cd-bpp bipyramidal one. However, higher densities of the gel are generally associated to strained crystals. The solvent composition is also important, as for example the 1/2 Cd-bpp bipyramids require at least a minimum amount of ethanol to appear. We demonstrated that in gel the strict "equality" stoichiometric criteria for metal-to-ligand ratios can be sometimes eluded, as non–equilibrium concentrations can be locally attained. In this respect, the crystallization geometry was proven to act as a key tool to influence the crystallization output, as it determines the direction and magnitude of the concentration gradients. Finally, the use of U tubes to perform one-pot screenings of a large part of the crystallization space is discussed.

Keywords: coordination polymers; crystal growth; gel growth technique; crystal morphology

1. Introduction

Understanding the outcome of crystallizing organic and metal-organic compounds is still a largely unresolved mystery of synthetic chemistry [1]. Despite remarkable advances from the theoretical front [2], the problem has no general and satisfactory solution yet, neither will it likely reach it in the next years, due to the lack of a predictive theory for the crystalline state [3,4]. Nucleation and growth kinetics are at least as important as thermodynamics in determining crystallization outcomes as, in fact, is usually observed [5,6]. The main physicochemical variables (concentration, solvent composition and density, nature of interfaces) are often strongly intertwined with each other, thus making any change in one parameter to produce unexpected and not easily understood effects in the product mixture [7].

To investigate these factors infinite times, an exhaustive and systematic screening of crystallization conditions represents a rational approach to study the crystallization pathway. The resulting crystal phase diagram (CPD) [8,9] can be used to identify suitable conditions for nucleation and subsequent crystal growth [10,11], and define the domains of existence of competing crystalline phases [12,13].

This is especially true in the subject of crystal engineering and supramolecular chemistry. Within this field, coordination polymers (CPs) represent a well-known class of organic–inorganic hybrid compounds that display a variety of tuneable properties. potentially useful in several forefront research fields [14–17]. These polymeric systems consist of extended networks of metal ions (M) linked by organic multidentate ligands (L) as bridging connectors, and are usually simply obtained by a self-assembly process of the components induced by dissolving and mixing [18,19]. However, a tight and efficient control over the product architectures is still out of reach. In fact, in many cases, the same ligand/metal (salt) pair, under very slightly different reaction conditions, can afford different polymeric species characterized by different stoichiometries and arbitrary dimensionality and topology of the extended networks [20,21].

To achieve a better control of the crystallization output, crystallization in gel can be used. This method offers several advantages with respect to classical experiments in solution, as in gel all the diffusion processes are slowed down and fluctuations are hampered, meaning that concentration gradients can be finely tuned [22]. However, before this method can be extensively applied, it is mandatory to explore its potentiality in the reproducible design of known crystal phases, and to check its effect on the quality of the synthesized crystals.

For two components systems, like CPs, but also more simple electrolytic compounds, the ratio between the two reactants concentrations can deeply influence the kinetics of the process and it is responsible for the "equality range" criteria for precipitation [23]. In this case, a rational way to find the proper conditions of crystallization and highlight the stability zones in multiphase systems is to determine the CDP as function of [L] + [M] and L/M parameters (square brackets indicate molar concentrations of the ligand and of the metal) under different environmental conditions [24].

Here, we exploit gels as a tool to go a step further with respect to the static control of concentrations. We extend the experimental study of $CdCl_2$:bpp (bpp = 1,3-*bis(4-pyridyl)propane*, Scheme 1) CP system [25,26] by performing a phenomenological comparative analysis of the crystallization behaviour in both solution and gel substrate in response to a systematic variation of the crystallization conditions, including the growth technique and the experimental set-up. We aim at clarifying the role of key physicochemical variables in determining the chemical nature and the morphology of the final crystallization products. Finally, we report for the first time an extensive mapping of the Cd-bpp phase diagram, in the context of exploring the effect of gel media on the composition of the equilibrium phase mixture, and on the morphology of the crystals. Due to the scientific and technological relevance of CPs, we hope to add a new powerful tool to the crystal engineer or materials scientist looking for new crystalline phases or new effective methods to produce the desired CPs with controlled morphology and crystal quality. In this respect, gel diffusion techniques, in varied experimental configurations, can become the method of choice due to their versatility. However, owing to the limited number of studies appeared so far, more details must be understood about the role exerted by gels upon crystal quality and their potential help for selecting the desired polymorphs or reticular isomers.
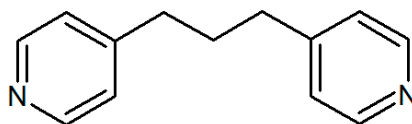
Scheme 1. bpp = 1,3-bis(4-pyridyl)propane.

2. Materials and Methods

All reagents (metal salt: $CdCl_2$ $2.5H_2O$; ligands: bpp = 1,3-bis(4-pyridyl)propane), agarose gel (EEO 0.09-0.13, gel point 36 °C, gel strength ≥ 1200 g/cm^2 at 1% gel and solvents (ethanol) employed were commercially available, obtained as high-purity materials from Sigma-Aldrich S.r.l. (Milano, Italy) and were used as supplied without further purification. Only the bpp ligand was purified by sublimation. Optical micrographs were recorded using a polarizing SZX16 Olympus stereomicroscope (Olympus Italia S.R.L., Segrate (MI), Italy) equipped with a digital camera for single shot or time sequence images acquisition. X-ray powder diffraction patterns were collected on a Philips PW 3050

vertical-scan diffractometer (Panalytical, Almelo, The Netherlands) X-ray single crystal data collections, for unit cell determinations, were performed at 293 K on a Bruker SMART Apex diffractometer equipped with a CCD detector (Bruker AXS, Madison, WI, USA).

2.1. Determination of Crystal Phase Diagram (CPD) in Solution

A broad screening of crystallization conditions in solution as a function of reactant concentrations ([M] = metal salt, $CdCl_2$ $2.5H_2O$; [L] = bpp ligand) and water-ethanol solvent mixture composition (*v/v*%) was carried out by using batch technique [27] in order to construct the relative crystal phase diagram [28]. Crystallization trials were rapidly set-up in a polypropylene 24-wells plate and air-tightly sealed with a 22 mm diameter glass cover slip and vacuum grease. A set of solutions of metal salt and bpp ligand at different concentrations were prepared in deionized water or ethanol. Crystallization trials were performed by mixing the appropriate amount of reagent solutions and pure solvent to reach a final volume of 2.0 mL for each fixed concentration of the components ([M], [L], EtOH %). The samples were kept at constant temperature (T = 25 °C ± 0.5) in a thermostat. The concentrations of metal salt and bpp ligand were systematically varied along the rows and the columns of the well plate. The samples were monitored by using an optical microscope coupled to a CCD camera, until equilibrium conditions were reached.

Two separate sets of crystallization conditions were investigated: a) total concentration of reactants (10 mM < [L] + [M] < 60 mM) and ligand-metal molar ratio (1.0 < [L]/[M] < 4.0), keeping constant the percentage of ethanol in the solution (50 *v/v* %). b) Volume content of ethanol (10 < EtOH *v/v*% < 50) and ligand-metal molar ratio (1.0 < [L]/[M] < 4.0), keeping constant the overall concentration of the reactants ([L] + [M] = 20 mM).

Powder samples were also prepared by fast precipitation from highly concentrated solutions of the reactants, either in water or in a mixture of H_2O-EtOH (50–50 *v/v*%) (see Supporting Information-section S1 for details). The nature and purity of the products formed by crystallization or precipitation were checked by single crystal diffraction or XRPD analysis by comparing the experimental patterns with the simulated ones from the single crystal structures.

2.2. Crystallization Screening in Gel (Single Diffusion Technique)

A broad crystallization screening in gel for the binary $CdCl_2$-bpp system was accomplished using the single gel diffusion technique [24,29]. Agarose was used as gelifying agent to avoid changes in pH or ionic strength and the presence of extraneous substances related to the gel-forming process. All the crystallization trials were performed in a glass tube (Ø 5 mm and 130 mm long).

2.2.1. Two-Layers Method (Water-Ethanol Solvent System)

A solution of cadmium chloride hydrate ($CdCl_2$ $2.5H_2O$) of desired molarity in double distilled water was mixed to an appropriate amount of agarose powder and heated up to boiling point, under stirring, until agar was dissolved. The hot solution was poured in a test tube (half test-tube, about 3.5 mL) and left to cool to ambient temperature. Gelation took place when the temperature fell below the gelling temperature (T_g = 36 °C). After gel setting, an ethanolic solution of specific molarity of bpp ligand (half test-tube, about 3.5 mL) was poured over the gel medium. The samples were kept at constant temperature (T = 25 °C ± 0.5) in a thermostat. A designed set of crystallization trials was carried out to screen a large variety of crystallization conditions. The ranges of parameters explored were as follows: gel concentration (0.1%, 0.5%, 1%, 3% *w/v*), initial total concentration of reactants (10 mM < [L]+[M] < 60 mM), ligand-metal molar ratio (1.0 < [L]/[M] < 3.0), with ligand and metal concentrations ([L], [M]) ranged from 5 to 30 mM.

A visual monitoring and scoring of crystallization trials were performed by optical microscopy at least once weekly for five weeks and, thereafter, occasionally until no changes were detected in the system. For each test condition, the following features were examined: phases and their approximate amount, spatial distribution along the tube, size and morphologies of the crystals.

Phases assignments were verified also by using X-ray diffraction techniques checking the nature of any observed morphology by comparison of the experimental data with the lattice parameters of the known crystallographic structures. Batch of crystals or crystals aggregates of each selected sample were extracted from gel and subjected to diffractometric analysis, either in single crystal or polycrystalline powdered form.

2.2.2. Three-Layers Method (Water-Ethanol Solvent System)

Crystallization trials were performed by using the same procedure described above (Section 2.2.1) except for a layer of pure gel sandwiched between the two layers of reactants. After gelation of the aqueous solution containing the metal salt ($CdCl_2 \cdot 2.5H_2O$) and the agarose powder (about 3.0 mL), a second layer of pure gel was created by adding about 1 cm of pure gel solution on the top of the $CdCl_2$-gel column. The buffer of pure gel was prepared at the same concentration of the first layer and cooled below 60 °C before the pouring. After the neutral gel layer was set, an ethanolic solution of specific molarity of bpp ligand (about 3.0 mL) was added carefully without disturbing the gel surface. The samples were kept at constant temperature (T = 25 °C ± 0.5) in a thermostat. A designed set of crystallization trials was carried out to screen a selected parameter space of crystallization conditions. The ranges of parameters explored were as follows: gel concentration (0.1%, 0.5%, 1%, 3% *w/v*), initial total concentration of reactants (20 mM < [L] + [M] < 40 mM), ligand-metal molar ratio (1.0 < [L]/[M] < 3.0), with ligand and metal concentrations ([L], [M]) ranged from 10 to 30 mM.

The monitoring of the crystallization trials over time and the identification of the crystal phases were performed as described above for the analogous screening (see Section 2.2.1).

2.2.3. Two-Layers Method (Water-Water Solvent System)

Gel was prepared by heating an aqueous solution of bpp ligand and the gelling agent (agarose powder) at the desired molarity up to boiling point under stirring until a clear solution was obtained. The hot solution was poured in a test tube (half test-tube, about 3.5 mL) and left to cool. The gelation process took place upon cooling to ambient temperature (gelling point, T_g = 36 °C). After gel setting, a solution of specific molarity of cadmium chloride hydrate ($CdCl_2$ 2.5H_2O) in double distilled water (half test-tube, about 3.5 mL) was poured over the gel medium. The system were allowed to evolve at constant temperature in a thermostat until equilibration (T = 25 °C ± 0.5). A designed set of crystallization trials was carried out to screen a large variety of crystallization conditions. The ranges of parameters explored were as follows: gel concentration (0.1%, 0.5%, 1%, 3% *w/v*), initial total concentration of reactants (10 mM < [L] + [M] < 60 mM), ligand-metal molar ratio (1.0 < [L]/[M] < 3.0), with ligand and metal concentrations ([L], [M]) ranged from 5 to 30 mM.

The monitoring of the crystallization trials over time and the identification of the crystal phases were performed as described above for the analogous screening (see Section 2.2.1).

2.3. Crystallization Screening in Gel (Double Diffusion Technique)

A high throughput crystallization screening in gel for the binary $CdCl_2$-bpp system was performed by double diffusion gel technique [22,24]. The crystallization experiments were carried out by using U-shaped tubes (Ø 4 mm and 100 mm long with two identical arms of 30 mm length) filled up with agarose gel. Gel solution was prepared by adding agarose powder to the H_2O-EtOH binary solvents system at the desired concentration and then heating the mixture until boiling. The hot solution (~2.8 mL) was poured in the U-tubes until the horizontal arm was filled and then the gel was allowed to set. After cooling, solutions of the reagents (~0.8 mL) of the appropriate concentrations were layered above the gel on the opposite arms of the tubes. To demonstrate the reproducibility of the results, some experiments were repeated two times. All samples were kept at constant temperature (T = 25 °C ± 0.5) in a thermostat and constantly monitored by using an optical microscope coupled to a CCD camera, until equilibrium conditions were reached.

A series of crystallization screenings were performed by fixing some boundary conditions (metal to ligand molar ration, U-tube size, total volume) and examining some specific parameters (total concentration, % ethanol, gel density). Values and range of the parameters used in this study: initial total concentration of reactants (25 mM < [L] + [M] < 90 mM), ligand-metal molar ratio (0.5 < [L]/[M] < 1.5), EtOH *v*% in the water-ethanol mixture (44%, 30%, 22%, 15% *v/v*%), gel concentration (0.1%, 0.5%, 1%, 3% *w/v*). The reactants concentrations were calculated by assigning half of the total volume of the tube to each components.

The monitoring of the crystallization trials over time and the identification of the crystal phases were performed as described above for the screening in test tubes (see Section 2.2.1).

2.4. Kinetic Growth Study

The kinetic experiments were performed by using a home-made optical cell consisting of two 2.6 $\times$ 7.6 cm^2 glass plates separated by a U-shaped rubber film 0.15 mm thick and 0.6 mm wide. The cell was half-filled with a warm ligand (bpp) aqueous solution containing agarose. Once the gel was cooled and set, an aqueous solution of metal salt (CdCl$_2$·2.5H$_2$O) was added until the cell was filled. After closing the upper edge of the cell with an adhesive tape, the sample was placed under a stereoscopic microscope (Olympus SZX16) equipped with a CCD camera (Lumenera Infinity 1-3C) (Teledyne Lumenera, Ottawa, Canada) and a time-lapse video recorder. The images were acquired with a decreasing temporal sampling rate over time and analysed using the Infinity Analyze software (version 6.0.0). Linear variations of the crystals size over time were measured on the video and converted to the real value by using a previously determined calibration factor. Two growth experiments were accomplished by using the same configuration and crystallization conditions except for gel density: [L] = 20.0 mM, [M] = 10.0 mM, [L]/[M] = 2, agarose gel 1.0% (Video S1), 0.1% (Video S2).

3. Results and Discussion

The present study focuses on a simple metal-ligand system, namely CdCl$_2$·2H$_2$O-bpp (hereinafter Cd-bpp, bpp = 1,3-*bis*(4-*pyridyl*)*propane*), that was well characterized some years ago by some of us with X-ray crystallography [26,30]. In particular, we investigated the crystal structure of the polymeric products obtained in different solvents (water, water/MeOH and water/EtOH) and reported some preliminary results of gel effect on the equilibrium composition, the morphological features of the crystals and the growth kinetics.

Despite small changes in the crystallization conditions, three different Cd-bpp solid forms can be obtained, all neutral but featuring different stoichiometries, topologies and crystal morphologies (see Table 1). Thanks to their peculiar crystal habits, such phases can be easily identified by visual inspection or optical microscopy. However, it remains to be understood what factors are determinant to produce a given phase composition at equilibrium.

Table 1. Cd-bpp coordination networks studied in this work. See also [26,30,31].

| Label	Formula	CCDC Number	DimensionAlity	Topology	Morphology	
3D-*dia*	[Cd(bpp)$_2$Cl$_2$]·*solv*	761818 CUPLIJ	3D, 4-fold	*dia* (6^6)	bipyramid	
3D-*sra*	[Cd$_2$(bpp)$_3$Cl$_4$]	604092 REMMIG [31]	3D, 2-fold	*sra* (4^2.6^3.8)	needle (aggregate)	
1D-*cha*	[Cd(bpp)$_3$Cl$_2$]·*solv*	761814 CUPKOO	1D	*zig-zag* chain	plate	

3.1. Crystallization in Solution

We first performed batch crystallization experiments (Figures 1 and 2) to check the behaviour of the system under conditions of high and constant supersaturation and in the absence of relevant concentration gradients. In a batch experiment, the supersaturation is achieved immediately upon mixing of the reactants. Thus, the kinetics of precipitation and equilibration are both very fast. The equilibrium or crystal phase diagram (CPD) in 50 % *v/v* aqueous EtOH solution (Figure 1) shows a wide field of coexistence of the *dia* and *sra* phases, with an increasing dominance of the first one as the [L]/[M] molar ratio increases. The *dia* network is the unique stable phase over a compositional range that largely depends on the total concentration of the reactants ([L]/[M] > 3.5 for 25 mM < [M] + [L] < 40 mM and [L]/[M] > 2.25 for [M] + [L] = 10 mM). On the contrary, crystalline *sra* can be isolated only in a narrow compositional range, i.e., at both very low total concentration and low molar ratio of the reactants. These results clearly reflect the chemical composition of the two polymeric systems characterized by a slightly different ligand content (*sra*: [L]/[M] = 1.5; *dia*: [L]/[M] = 2). Under these conditions, crystal morphologies are essentially unaffected by composition. The 3D-*sra* phase usually appears as powder, clusters of thin needles or spherulites, while the *dia* system invariably exhibits a well-formed bipyramidal crystal habit.
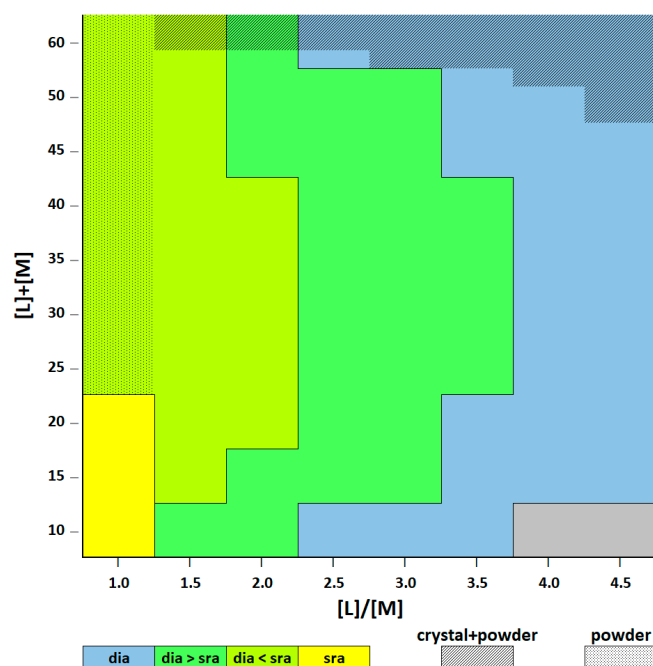
Figure 1. Equilibrium phase diagram for aqueous EtOH solutions (50 vol%) of the CdCl$_2$-bpp system, with indication of the stability regions for 3D-*sra* and 3D-*dia* polymers as a function of [L] + [M] total concentration and [L]/[M] molar ratio (M = Cd^{2+}, L = bpp).

On the contrary, when the solvent composition was allowed to vary, the picture changed. We systematically modified the volume content of EtOH at different metal-ligand molar ratios (1.0 < [L]/[M] < 4.0), while keeping constant the overall concentration of the reactants ([L] + [M] = 20 mM). The phase diagram (Figure 2) clearly shows how a minimum amount of ethanol is required to observe the formation of the *dia* phase (>10%). Conversely, the 1D polymer *cha* can only be obtained in pure water or in EtOH/H$_2$O mixtures at quite low ethanol concentration (lower than ~20%). As expected, the stability regions of the different species correlate with their stoichiometric composition, showing the dominance of *sra* phase at low [L]/[M] ratio, although the phase boundaries are well defined only for the 1D-*cha*:3D-(*sra* or *dia*) transition. Actually, competition and coexistence between the 1D-*cha* and 3D-*sra* phases have been observed in more concentrated aqueous mixtures

of the reactants ([L] + [M] > 30 mM). To prepare pure powder samples of the two products by using water as single solvent, a stoichiometric excess of one component is invariably required, namely an excess of ligand for the 1D-*cha* polymer and an excess of metal salt for the 3D-*sra* species (see Materials and Methods, Section 2.1 and Supporting Information S1).
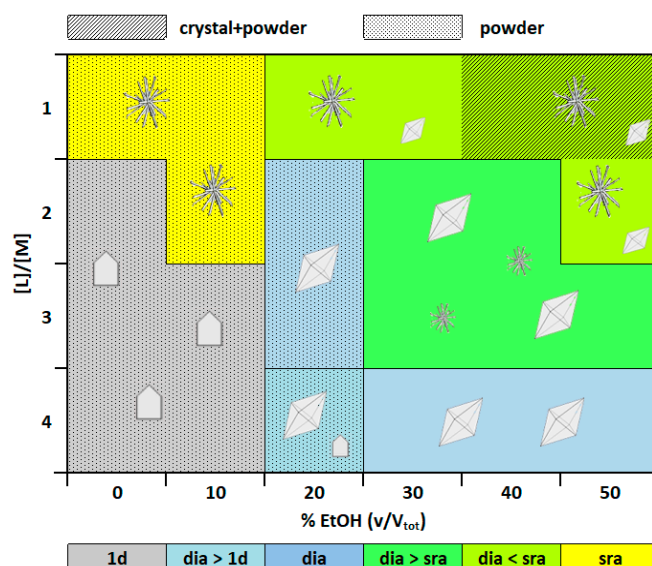
Figure 2. Equilibrium phase diagram for aqueous EtOH solutions of CdCl$_2$-bpp system at a 20 mM total concentration of the reactants, with indication of the stability regions for 3D-*sra*, 3D-*dia* and 1D-*cha* species as a function of [L]/[M] molar ratio and the solvent composition (M = Cd^{2+}, L = bpp).
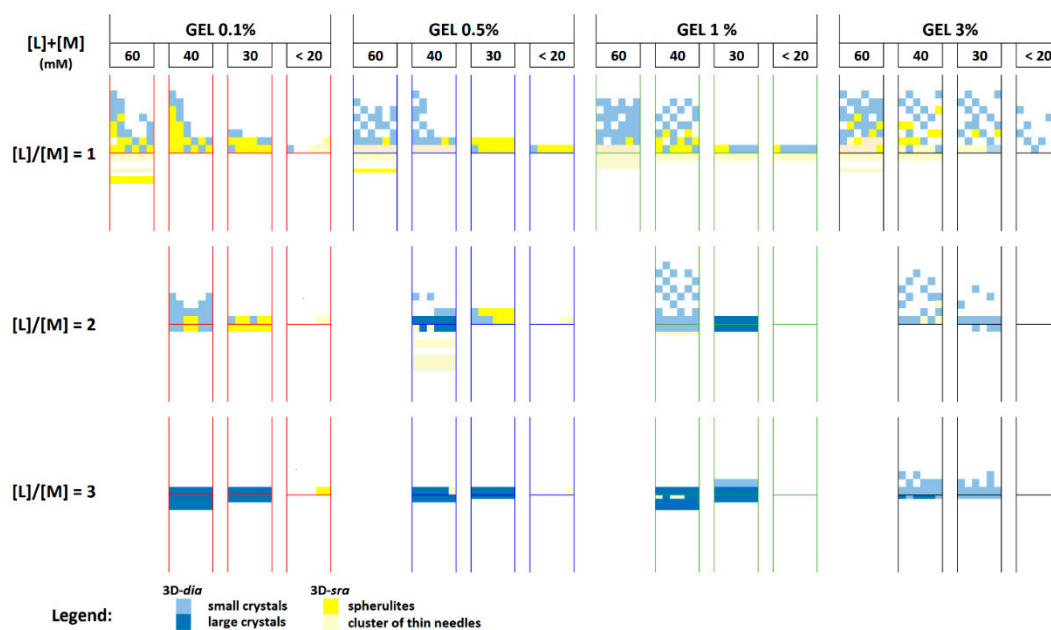
3.2. Crystallization in Gel

When kinetic effects come into play, i.e., when the equilibration rate is relatively slow, the formed crystals might exploit different phase compositions and morphologies compared to those obtained from batch/solution experiments. In this respect, gel-based crystallization techniques can improve size, quality and mechanical stability of crystals of coordination polymers, as well as induce structural alterations in the macro and micro morphologies of these materials [32,33]. The capability of gel media to promote selective crystallization of polymorphs or to stabilize metastable phases [34,35] by acting on the nucleation kinetics is also well known. This makes it possible to consider the gel method as a general and useful way to modify the relative stability of correlated crystal forms or generate new crystalline solids.

To explore further the crystallization kinetics of Cd-bpp systems, we transferred some batch trials to diffusion conditions, by using the reaction single diffusion technique to perform a comprehensive screening. We have chosen agarose gel media as diffusive dispersion matrix in order to avoid changes in pH or ionic strength and the presence of extraneous substances connected to the gel-forming process (see Materials and Methods, Section 2.2).

3.2.1. Crystallization in Water-Ethanol Solvent System

Layering of an ethanolic solution of the ligand over an agarose-gelified aqueous solution of the metal salt (see Materials and Methods, Section 2.2.1) generates counter-diffusion of both reactants and solvents, resulting in a complex precipitation profile. However, the total reactant concentration ([L] + [M] = 60, 40, 30, < 20 mM), the molar ratio of the reactants ([L]/[M] = 3, 2, 1) and the gel composition (0.1%, 0.5%, 1%, 3% *w/v*) proved to be key parameters to highlight coherent trends. Figure 3 summarizes the main outcomes. We selected a graphical layout that allows to appreciate at a glance (i) the phase composition at equilibrium, (ii) the phase front distribution along the tube, (iii) the size and (iv) the morphologies of the crystals.

Figure 3. Summary of results of the crystallization screening performed by using the two layers-gel technique (in water-ethanol) for CdCl$_2$-bpp. The stability regions of the different species are shown as a function of [L] + [M], [L]/[M] and gel strength parameters (M = Cd^{2+}; L = bpp). The phase distribution along the tube is also shown.

Two patent differences with respect to the batch crystallization experiments (see above) stem from Figure 3. First, the 1D-*cha* phase is now missing even in a large excess of bpp ([L]/[M] >> 1), restricting the competition in the arena of the phase equilibria to 3D networks only. Second, higher supersaturation levels are generally required for nucleation, as in most cases no crystals are obtained at low (< 20 mM) [L] + [M] reactantsconcentrations.

When the overall concentration of the reactants [L] + [M] increases (Figure 3, from right to left for each gel strength), the amount of precipitated material increases as well, but it is essentially independent from the [L]/[M] ratio (Figure 3, vertical axis). However, higher [L]/[M] values definitely favour the 3D-*dia* species over the 3D-*sra* one, allowing the formation of fewer crystals of larger size. This behaviour reflects the different stoichiometry of the two phases, as confirmed by their relative and absolute spatial distribution. In fact, the *sra* product, when present, is always located below the *dia* crystals, in a zone richer in metal salt. In all trials, precipitation starts at the solution/gel boundary, then the reaction front moves upward (M in water/gel) faster than downward (L in ethanol) favouring the crystallization in the supernatant solution and the formation of 3D-*dia* system, which requires higher [L]/[M] ratios. Only at very high [L] + [M], the diffusion profile allows to observe nucleation of the *sra* phase in the gel matrix, below the sol-gel interface (Figure 3, left).

The number of nucleated crystals, as well as their size and morphology, is mostly controlled by the gel composition. An increase of the gel density (Figure 3, from left to right) corresponds to a decrease of the pore size that slows down the diffusion of reactants, in turn reducing the speed at which linear concentration gradients are set up. The supersaturation is thus obtained in longer times, but its magnitude is generally higher than in low-density media. Accordingly, when the most concentrated gel is used (3% *w/v*), many more crystals are formed in the supernatant aqueous solution, where faster supersaturation can be achieved. Thus, fewer crystals are present at the interface, with a markedly smaller average size, as they nucleate in a higher supersaturation regime. At the opposite end of the composition axis, low-density gels (0.5% and 1% *w/v*) allow nucleation of diamantoid-3D polymers at the solution/gel interface. Such crystals conserve their characteristic bipyramidal shape, but their lower part, growing in the gel, is significantly tapered and warped. However, despite of the compressive stress action of the gel, they maintain their single-crystal nature but, unfortunately, do not seem to

give rise to gel-trapping phenomena (Figure 4). Gel incorporation phenomena is an important aspect to consider because it is responsible for the generation of biomimetic composite crystals with large porous internal structures as well as specific superstructure and characteristic textures at the micro or nano scale, similar to those observed in nature [36]. Moreover, as shown in our previous work for a flexible porous network [37], due to gel inclusion, highly porous materials can show an extremely improved mechanical stability and resistance to dehydration giving crystals of lower mosaicity and higher diffraction quality [38].
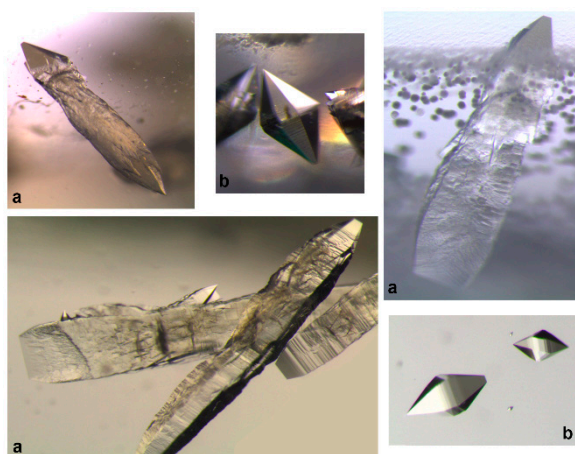

Figure 4. (**a**) Crystals of 3D-*dia* grown at the solution-gel interface. The bottom part of the crystals, grown in gel, appeared clearly warped with an elongated shape. (**b**) Crystals of 3D-*dia* grown in solution with a well-defined bipyramidal morphology.

The 1% *w/v* crystallizing medium lies somewhat in the middle, as it allows clusters or individual well-defined plates of 3D-*sra* to appear in gel at low-to-intermediate [L]/[M] values (Figure 3), and fewer but larger crystals of 3D-*dia* at the interface at higher [L]/[M] ratios.

3.2.2. Addition of an Intermediate Layer of Pure Gel

The presence of an intermediate layer of pure gel between the reactants chambers ("buffering") prevents the direct contact between the reagents, thus reducing the initial supersaturation with respect to previous experiments (see above). As diffusion takes place in a finite time across the buffer layer, the overall kinetics of the process is affected, resulting in different equilibrium compositions and phase distributions with respect to experiments described in Section 3.2.1. The relevant outcomes are shown graphically in Figure S1 (in Supplementary Materials). The most striking effect is a severe hampering of the precipitation in the solution layer, while the phase boundaries described above shift downward: most of the material crystallizes at the solution/gel interface with a clear preference for the 3D-*dia* species. Most important, the 3D-*sra* phase appears in the gel matrix in the majority of trials, including those in which the [L]/[M] ratio is apparently unfavourable (3:1). Moreover, the gel concentration has little or no effect on the yield of the crystalline material: a small change was detected only using the strongest medium (3% w/*v*).

By contrast, several significant macro-morphological modifications occur for crystals entirely grown inside the gel but above specific gel-density levels. In particular, the radiating arrays of acicular crystals typical of 3D-*sra* product change to spherulites, axialites or aggregates of lamellar units and very small platelet crystals, depending on the crystallization conditions (Figure 5). The bipyramidal 3D-*dia* crystals instead are strongly deformed and produce disordered aggregates or intergrown crystals.
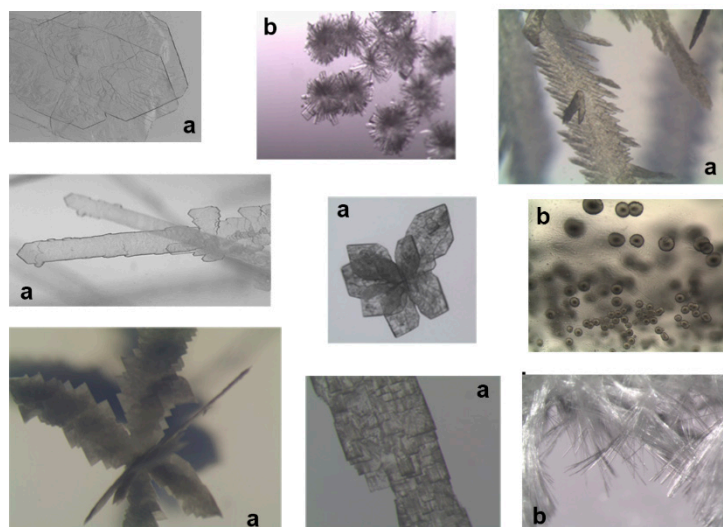
Figure 5. Different morphologies observed for the crystals of 1D-*cha* (**a**) and 3D-*sra* (**b**) species.

We would like to stress the role of gel in determining a large morphological variability at several hierarchical levels including crystal aggregation and morphology alteration phenomena. This is because the habit of the crystalline materials, but also the microscopic structures of the crystals, can have a strong influence on their many properties and functions. Beyond the morphological effects, the gel matrix is responsible for periodic precipitation phenomena observed in reaction diffusion systems involving mainly electrolytic compounds [39]. The features of these precipitation patterns and the transition between periodic or tubular precipitation, dendritic crystal aggregates and well-formed crystals, have been explained by considering the nature, the chemical quality and the concentration of the gelling agent [40,41]. The correlation between crystallization conditions and the over-organization of the crystalline precipitate is important to clarify the mechanistic aspects involved in their generation. This is a matter of great importance because pattern-forming phenomena are ubiquitous in nature especially in geological and biological process [42]. However, no satisfactory explanation has still been provided for their development [43]. In addition to the study of the mechanism, pattern formation in precipitation process including the growth of dendritic nanostructures has gained great interest in material science because can serve as basis in development of meso, micro and nano-devices [41].

3.2.3. Crystallization in Water-Water Solvent System

To understand the role of ethanol in determining the phase diagram, we have performed a crystallization screening analogous to those described in Section 3.2.1 by using water as solvent for both components and switching the position of the two reactants, i.e., metal salt solution layered over a gelified solution of the ligand. We considered overall starting concentrations of the reactants [L] + [M] = 60, 40, 20, < 10 mM, in conjunction with molar ratios [L]/[M] = 3, 2, 1 and gel strengths of 0.1%, 0.5%, 1%, 2%.

Figure 6 summarizes the results. As in the water/EtOH system, the stoichiometry of the observed products closely matches the concentration profiles generated by the counter-diffusion of reactants through the gel-solution column. The most striking difference with respect to previous experiments is the absence of the 3D-*dia* phase, which clearly requires a minimum amount of ethanol to form. On the contrary, the 1D-*cha* network, which was completely absent before, is now the predominant product.
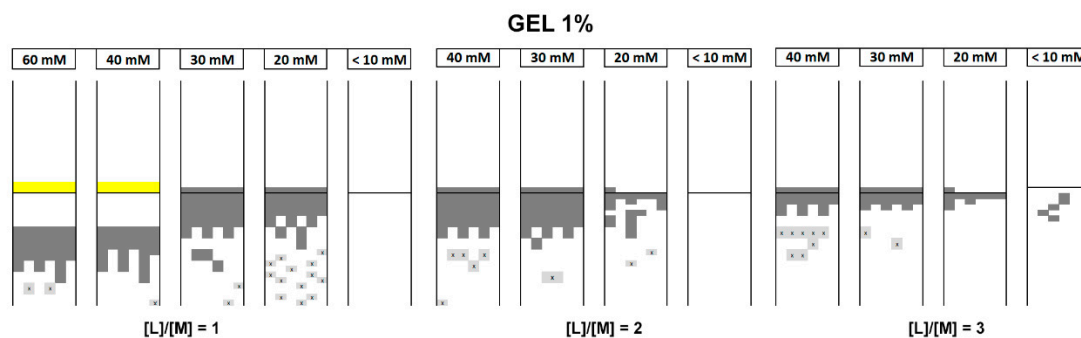
Figure 6. Results of the crystallization screening performed by using the two layers-gel technique in water for CdCl$_2$-bpp. This representation shows the stability regions of the different species as a function of the starting total [L] + [M] reactant concentrations and [L]/[M] ratio (M = Cd^{2+}; L = bpp), as well as also the phases distribution along the tube. Yellow = 3D-*sra* phase (thin needles); dark grey = 1D-*cha* phase (big dendritic "fern-leaf" shape); light grey−(x) = bladed or radial aggregates of platy 1D-*cha* crystals.

The 1D-*cha* species grows in form of dendritic crystals extending downward from the nucleation sites at the liquid-gel interface (Figure 7). Only at higher depth in the gel, flower-like aggregate of plates of the same phase appear.

Figure 7. Crystallization trials close to equilibrium performed by using the two layers-gel technique at [L] + [M] = 28 mM and varying [L]/[M] ratios (M = Cd^{2+}; L = bpp). All the crystals belong to the 1D-*cha* phase. The number of crystals and the depth at which they form decrease while increasing the ligand to metal molar ratio. Only the half of the tubes filled with gel are shown.

Actually, both the [L] + [M] and [L]/[M] parameters deeply affect the final architecture of the aggregated 1D-*cha* crystals, which move from an irregular dendritic "fern-leaf" shape to bladed or radial aggregates of large or thin platy crystals at high [L] + [M] and low [L]/[M].

The overall crystallization yield of 1D-*cha*, as well as the distance of the crystals from interface at equilibrium, increase with the [L] + [M] parameter but also with the reduction of the [L]/[M] one (Figures 6 and 7). This is rather surprising, as the stoichiometry of this complex requires three times the molar amount of the ligand per metal centre (Table 1) but it can be explained by taking into account the different diffusion mobility of the two components, the stoichiometry of the products and the higher supersaturation required in gel to observe nucleation.

Under these conditions, a significant supersaturation is achieved throughout the gel, determining the nucleation and growth of the 1D-*cha* product. Then, the equilibrium is continuously shifted toward

1D-*cha*, as all the transport phenomena are slowed down in the gel medium and the spatial/time evolution of the two concentration profiles is different.

The competing 3D-*sra* phase can only appear in the supernatant for [L]/[M] = 1, but requires higher values of [L] + [M] compared to crystallization from solution (Section 3.1). 3D-*sra* grows at the sol-gel interface, almost 0.5 cm above the 1D-*cha* species, and forms aggregates of well separate needles that extend upward (Figure 6).

The system is essentially unaffected by changes in gel stiffness in terms of composition, amount of crystalline material and overall morphology. Only for low-density gel (0.1 *w/v*%) relevant morphological changes have been detected consisting of a clear reduction in the gel-induced deformations of the crystals. Moreover, a fast evolution of the crystals shape during the growth process until obtaining the typical sword-shaped morphology of 1D-*cha* species has been observed (Figure S2). To highlight the changes in the growth mechanisms responsible for the phenomena, an in-situ kinetic study has been performed (see Section 3.4).

3.3. Crystallization by Double-Diffusion Method in U-Tube

We performed a further crystallization screening with the double-diffusion gel technique in water-ethanol mixtures (see Materials and Methods, Section 2.3). Within a U-tube, the horizontal column of gel acts as a neutral separation buffer, allowing a finer control of the double-diffusion of reactants. Therefore, the [M] and [L] concentration profiles change continuously not only in space, but also in time, generating a time-dependent gradient of supersaturation along the diffusion path. This implies a continuous change of both [L] + [M] and [L]/[M] parameters, and determines a spatio.temporal sequence of crystallization events that depends on the thermodynamic boundary conditions. To avoid complex correlations, we chose to fix the parameters U-tube size and total volume to test the effect of those defining the main chemistry of the crystallization environment ([L]/[M], [L] + [M], EtOH %, gel density). The experimental outcomes, including the time response of the system, are shown in Figure 8.
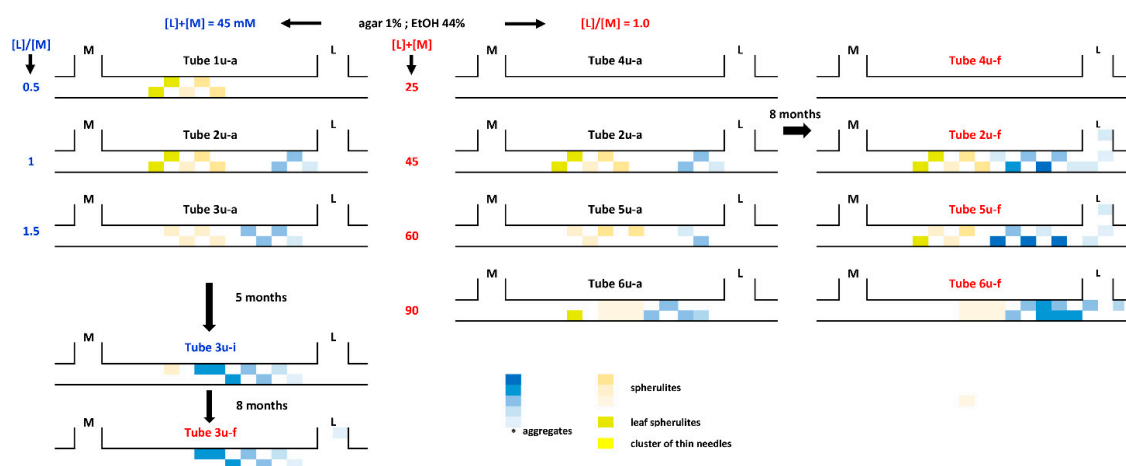
Figure 8. Results of the crystallization screening in water-EtOH 44% *v/v* performed by double diffusion in a U-tube for the CdCl$_2$-bpp system. The schemes refer to a growth period of five weeks. The effect of [L] + [M] and [L]/[M] is shown at constant solvent composition and gel density with fixed boundary conditions (U-tube size, total volume). The month-scale time evolution of the crystallization trials is also reported, to highlight the long time required to reach equilibrium.

3.3.1. Concentration of Reactants

As expected, no precipitation is present below a concentration threshold (~45 mM) roughly similar to that required in the test tube trials; as before, the spatial distribution along the gel column of the different compounds reflects their [L]/[M] composition.

In most trials, new crystals nucleate continuously, but growth of the 3D-*dia* species is favoured (see Figure 8 and Figure S3). Therefore, a large number of crystals is present at equilibrium, with a non-homogeneous size distribution. The morphology of the products is markedly different with respect to solution-grown crystals, due to the gel matrix. In particular, the 3D-*dia* bipyramidal crystals acquire an entirely elongated shape, with rounded edges and a rugged surface. For this species, phenomena of disordered intergrowth and aggregation of crystals have been also observed. For the 3D-*sra* compound, only the spherulitic habit is adopted under these conditions.

Equilibration invariably requires long times, of the order of months. However, specific timescales and kinetics strongly depend on the growth conditions. High [L] + [M] concentrations induce larger observable changes during equilibration, while high [L]/[M] ratios enhance the transformation rate in the starting stage (Figure 8). More in detail, an increase of the [L]/[M] ratio increases the precipitation yield and, according with the stoichiometric composition of the products, the formation of the 3D-*dia* over the 3D-*sra* phase. On the contrary, when [L] + [M] is raised at constant [L]/[M] = 1/1, the precipitation yield is only barely increased, but the precipitation area undergoes a marked narrowing, without variation in the relative composition of the system.

3.3.2. Chemical Environment

Experiments have also been undertaken as a function of solvent composition (EtOH: 44, 30, 22, 15 *v/v*%), gel concentration (3, 1, 0.5, 0.1 *w/v*%) at constant [L] + [M] and [L]/[M], to test the effect of the chemical environment on the crystallization of $CdCl_2$-bpp. Despite the limited sampling of the parameters space, interesting trends emerged, consistent with screenings in solution and gel (Sections 3.1 and 3.2). Results are reported graphically in Figures S4 and S5.

Concerning the solvent composition, as the water content is increased, the 3D-*dia* phase is more and more favoured over the 3D-*sra* one. At the same time, the precipitation zone widens and moves toward the ligand arm (L), while a large region of coexistence of the two 3D phases appears. Interestingly, the morphology of *sra* is very sensitive to the EtOH content and exhibits larger and larger varieties of morphologies as the amount of alcohol decreases. Going from the metal arm (M) to ligand arm (L) of the tube, small spherulites, rosette-like aggregates of radiating plates, and spherical clusters of thin needles are observed for dilute enough solutions. 3D-*dia* is instead much less affected. This phase essentially forms bow-tie aggregates of misshapen bipyramidal crystals and compact clusters of small parallel crystal units, near the ligand solution or the L-end of the tube. In addition, the size of the crystals increases as the EtOH percentage increases (see Figure S4). Only in the presence of pure water, i.e., at 0% EtOH content, the 1D-*cha* species appears, as observed in single diffusion trials (Section 3.2).

A change in the gel density (Figure S5) severely affects the crystal morphology, while the relative product yields and the total amount of precipitate, though undergoing significant changes as well, are less influenced. High concentrations of the gel favour the *sra* phase, at the expense of a slight decrease in the nucleation density. Even though aggregation phenomena and morphology alterations occur at any gel density, deformation effects are most evident in the densest medium (3% *w/v*). In this case, almost shapeless *dia* crystals are formed, while *sra* exhibits a huge variety of morphologies. A complete morphological range, consisting of a sequence of small and large spherulites, aggregate of radiating slender fibres and clusters of plates, has been spanned even in a single crystallization test.

3.3.3. Overall Parameters Analysis

A crosscheck between information provided by all crystallization experiments made it possible to highlight how the effect of the crystal growth parameters on the crystallization process are closely correlated. For example, in presence of a high ethanol content, the total concentration of reagents largely affects the spatial distribution of the products while at low alcohol percentage [L] + [M] influences the precipitation degree and the ratio between the products.

It is clear that the U-tube method allows a more cost-effective and faster screening of crystallization space compared to the other configurations. Moreover, U-tube trials highlight some peculiar features of

a two components M-L diffusing-reacting system in terms of stability and composition of ML_n products. However, the different mobility of the diffusing entities in gel as well as the time dependent evolution of the system in terms of concentration gradients and, therefore, of supersaturation along the gel column, are responsible for a more complex history-dependent precipitation profile and consequently for a distinctive, method-related phases distribution [44,45].

In fact, for a two components, diffusion-reaction configuration has been proven that, beside the critical supersaturation, the "equivalency" rule of the reagents activities must be fulfilled for nucleation to occur [23,24]. For this reason, time and location of nucleation events result strictly connected to both the solubility properties of the products and to their stoichiometric composition. Furthermore, the supersaturation level and its evolution toward the critical threshold can affect the growth mechanism in any stage of the growth process, resulting in clear morphological effects, like the generation of radial spherulites at high supersaturation degrees.

Our systematic study has highlighted how the evolutionary "history" of the system, that deeply influences the kinetics of the whole process, may be modified by simply changing the initial reagents' concentration, the solvent composition, that is the solubility products and the relative stability of the phases, or the gel density, that is the mobility of the diffusing components.

3.4. Kinetics of Growth

In the crystallization screenings in water performed in test tubes (see above), the nucleation takes place at the gel-solution interface as a result of an instantaneous reaction between the upper ($M = CdCl_2$) and lower ($L = bpp$) reactants, except at very low total concentration [L] + [M]. In most trials, crystals of the 1D-*cha* phase nucleate and grow downward very fast and continuously up to several centimetres in length. Beyond the effects on the system's composition and phases' distribution, due to the change of the crystallization conditions during the screening, we have detected relevant morphological effects (see above). The most important one is definitely the quite fast shape evolution process undergone by the 1D-*cha* crystals from an irregular dendritic shape towards the typical sword-shaped morphology of this species. To highlight the changes in the growth mechanism responsible for these phenomena, we have performed an in situ and real-time observation of the growth process by optical microscopy.

Since the gel stiffness can affect the characteristics and the diffusion properties of the gel network, we carried out two identical experiments using gels of different density (1.0 and 0.1 w/v %). The evolution of the crystals size and the relative growth rate profile as function of time for both investigations are reported in Figure 9, Figures S6–S8 and Figure 10, Figure 11 and Figure S9. In both cases, it is clear that the relaxation of supersaturation toward equilibrium occurs via different growth mechanisms, generating deep and characteristics morphological changes in the system.

In the first experiment (gel density = 1 *w*/v %), the crystals grew very fast, leading to dendritic structures with the typical fern-leaf shape observed during crystallization in gel for this species (see Section 3.2.3). We have collected and analysed data on three different crystals during the growth process. To reduce potential errors in the growth rate estimation arising from the manual evaluation of data and the irregular shape of the growing system, we measured the linear size of the crystals on the recorded images in different growth directions parallel to the focusing plane of the camera.

The frame sequence shown in the time-lapse Video S1 and Figure S8 illustrates the shape and size variation of the crystals and, above all, the progressive morphological evolution of the crystals revealing a "reverse" roughening transition indicative of a change in the growth mechanism. The initially "rough" surface of the crystal becomes more regular and smoother as supersaturation decreases and growth slows down, leading to the formation of a regular system of macroscopic steps. As growth proceeds, a lateral propagation of the steps takes place producing continuous layers and allowing a partial morphological recovery of the crystals [46,47].
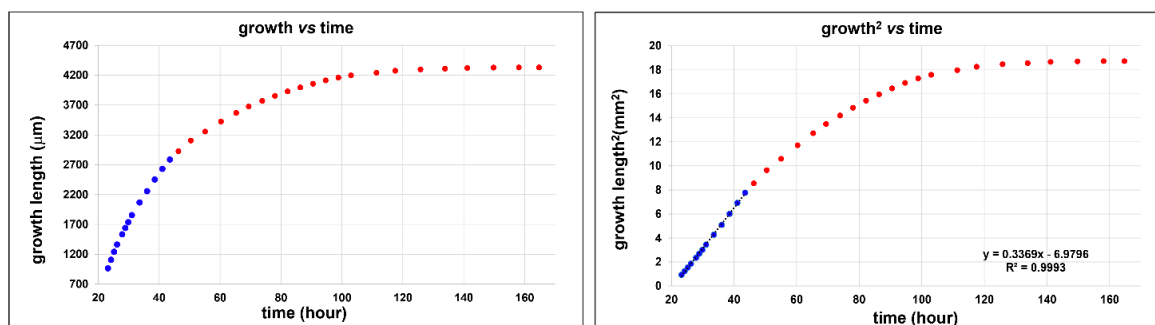
Figure 9. Measured values of the crystal size (**left**) and its square (**right**) plotted versus time for the middle and final stage of the growth process (23–164 hours, gel density 1 *w/v%*). The shape of the curve changes over time (blue and red dots) suggesting a change in the growth mechanism. Only some selected experimental data points have been reported for clarity. Dotted lines show the fitting of the data according to the relation reported alongside the curve. The linear size of the crystals in different growth directions parallel to the focusing plane of the camera has been measured. The absolute values are direction-dependent but the growth behaviour is the same for any directions.
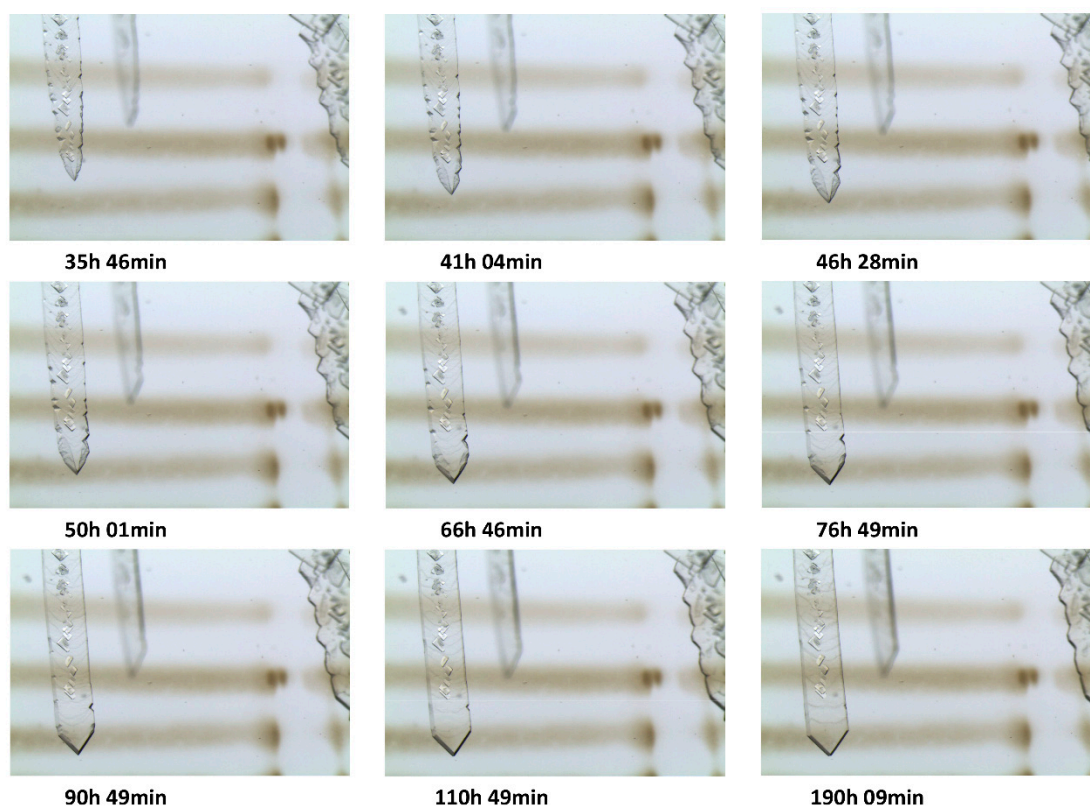

Figure 10. Optical microscopy images of the *morphology evolution* in the *time-dependent* crystal growth experiment of 1D-*cha* polymer (agarose concentration 0.1 *w/v %*). The images show the morphological evolution of the crystal from an irregular morphology to a well-defined sword shape.

This phenomenon can be explained by considering the strict correlation existing between supersaturation, growth mechanism, growth rate and the structural profile of the surface [48–51].

In order to determine the mechanisms involved in the growth process we should use the standard plot of the growth rate evolution as a function of supersaturation. However, in a diffusive reacting system like the present one, an accurate measurement of the time-dependent supersaturation in the close proximity to the crystal face is very complex and time-expensive. We have, therefore, performed a direct fitting of the experimental crystal size vs. time and discuss the results by using an appropriate

kinetic model to extract the mechanistic information and, above all, to highlight changes in the growth regime [49].
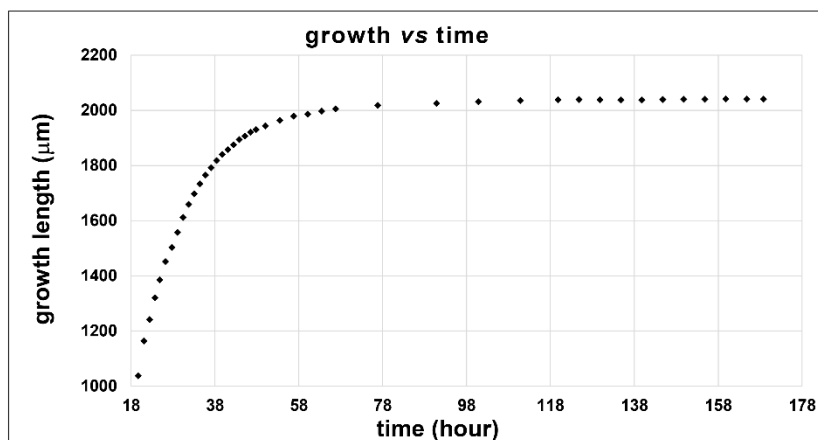
Figure 11. Measured values of the crystal size (crystal length from the tip of the crystal) plotted versus time for the middle and final stage of the growth process (20 to 168 hours, gel density 0.1 *w/v*%). Only some selected experimental data points have been reported for clarity. The crystal reconstruction seems to start about 40 hours after the experimental start-up (see also Figure S9).

Figure 9 and Figure S7 show the experimental results for the middle stage and the whole growth process, respectively. The initial portion of the curve in Figure 9 (L *vs.* t) is parabolic, as confirmed by the linear dependence of L^2 from the time of growth (see L^2 *vs.* t graph in Figure 9). This behaviour is usually considered characteristic of one-dimensional diffusion [46,48]. At a later stage of the growth, the curve is better described by a quadratic function that seems to suggest a growth mechanism controlled by surface integration. Whatever the mechanism, it is clear that a transition occurs between different growth regimes.

The second kinetic experiment has been carried out by using a low gel density (0.1 w/v %) in order to reproduce the morphological development observed in a single-gel diffusion crystallization trial (see Section 3.2.3 and Figure S2). The time-laps video S2 and Figure 10 show the growth of a crystal in real time from 5 to 170 hours after the experimental start-up. Figure 11 shows the analysis of the growth data relative to the crystal length measured from the tip of the crystal.

During the process, we have observed a notable morphological evolution of the crystal from an irregular pattern characterized by jagged lateral profiles to a well-defined sword-shaped morphology representing the common habit observed for the polymeric 1D-*cha* species under study (see Figure 11 and Figure S2). The crystal shape recovery takes place by enlarging the lateral "ledges", which mutually coalesce, and by the rebuilding of the crystal tip. The process starts when the growth rate becomes very low and the crystal lengths do not increase appreciably any more (after about 78 hours). In this case, we cannot speculate about the mechanism involved in the reconstruction route, because the growth data refer to the tip of the crystal, even though the measurements may be considered representative of the {110} faces. No data regarding the microstructural events involving the lateral irregularity can be measured at the optical microscope resolution. However, it is clear that the polyhedral form is (re)generated, as expected, at very low supersaturation, in a kinetic-controlled system near equilibrium where morphological stability is recovered.

4. Conclusions

In this work, we have shown the results of a thorough experimental screening on the crystallization behaviour in gel of a two-component (metal-ligand) diffusing-reacting system, forming three different coordination polymers featuring different topologies (3D-*dia*, 3D-*sra* and 1D-*cha*), crystal morphologies and various ligand to metal ratios. Through a phenomenological approach, we provided several

insights on the chemical, environmental and boundary conditions affecting the kinetics of the whole crystal formation process, including the equilibrium phase composition of the Cd-bpp system.

In this study, we have proven that the use of gels as reaction-diffusion media could dramatically alter the crystallization picture observable in solution. In particular, the gel composition can control number, size and morphology of the nucleated crystals while the crystallization geometry can deeply influence the direction and magnitude of concentration gradients, affecting the overall kinetics of the process and, thus, the crystallization outcomes. Of utmost importance, however, is the fact that the gel can easily allow the system to escape from strict "equality range" criteria, as far from equilibrium concentrations can be locally attained, which persist for a long time, due to lower diffusion rates. For example, needle-like crystals of the 3D-*sra* phase (L:M 3:2) can nucleate in the gel buffer, even when the nominal [L]/[M] ratio is apparently unfavourable (3:1). On the contrary, with a reversed sequence of the gel and solution layers in the crystallization column, the formerly missing 1D-*cha* plates become neatly favoured.

We also showed that experiments in a U tube constitute a cheap way to study the evolutionary "history" of the system, that is, the spatiotemporal sequence of phases that crystallize at different positions and times, while the concentration gradient of the reagents and, thus, the supersaturation profile, varies very slowly. This means that the U tube setup is particularly suited for one-pot explorations of the crystal phase diagram, as it allows to literally taking snapshots of the evolving product mixture as the diffusion of reactants proceeds. The continuous evolution of the concentration gradients is also demonstrated by measurements of the growth kinetics of the 1D-*cha* plates. Our measurements highlight a transition between diffusion–controlled and reconstructive growth regimes, as the system spontaneously switches from the first stage to the second one, depending on the relative amount of supersaturation.

We stressed the role of gel in determining deep morphological modifications, including crystals aggregation, morphology alterations and gel inclusion phenomena. This is because experimental evidence supports the hypothesis of a strong influence of these effects on the properties and functionalities of the crystalline materials, such as CPs, opening up new possibilities for their use in technological applications. Moreover, a detailed morphological analysis of aggregation phenomena in a reaction-diffusion system may be helpful to understand the pattern formation mechanism in diffusion-limited reaction that is common in biological and geological processes occurring in nature.

There are only a few examples in the literature of the application of gel growth technique to the synthesis of coordination polymers (CP) or metal-organic frameworks (MOF). However, some experimental studies of the morphological evolution of the system depending on specific experimental parameters (temperature, density of the gel and concentration and nature of the reagents) are available [52]. As in our case, the outcomes are always discussed in terms of generation of a supersaturation wave propagating through the reaction-diffusion systems [53,54]. All the results seem to support the hypothesis of a non-chemical action of the gel matrix that is essentially responsible of an efficient hindering of the rates of nucleation and crystal growth.

As a final remark, we think that crystal growth in gel is an effective tool to acquire a better understanding of the crystallogenesis process of CPs but also as method to induce macro and micro alterations in the morphologies of these materials and a useful way to modify the relative stability of correlated crystal forms.

Author Contributions: Conceptualization: S.R, M.M.; investigation: S.R.; writing—original draft preparation: S.R., L.L.; review: L.L., M.M.

Conflicts of Interest: The authors declare no conflict of interest.

References

1. Gavezzotti, A. Are Crystal Structures Predictable? *Acc. Chem. Res.* **1994**, *27*, 309–314. [CrossRef]
2. Neumann, M.A.; Leusen, F.J.J.; Kendrick, J. A Major Advance in Crystal Structure Prediction. *Angew. Chemie Int. Ed.* **2008**, *47*, 2427–2430. [CrossRef] [PubMed]
3. Desiraju, G.R. Crystal Engineering: A Holistic View. *Angew. Chemie Int. Ed.* **2007**, *46*, 8342–8356. [CrossRef] [PubMed]
4. Gavezzotti, A.; Presti, L. Lo Building Blocks of Crystal Engineering: A Large-Database Study of the Intermolecular Approach between C–H Donor Groups and O, N, Cl, or F Acceptors in Organic Crystals. *Cryst. Growth Des.* **2016**, *16*, 2952–2962. [CrossRef]
5. Gavezzotti, A.; Lo Presti, L. Dynamic simulation of liquid molecular nanoclusters: Structure, stability and quantification of internal (pseudo)symmetries. *New J. Chem.* **2019**, *43*, 2077–2084. [CrossRef]
6. Destro, R.; Sartirana, E.; Loconte, L.; Soave, R.; Colombo, P.; Destro, C.; Lo Presti, L. Competing C=O . . . C=O, C-H . . . O, Cl . . . O, and Cl . . . Cl interactions governing the structural phase transition of 2,6-dichloro-p-benzoquinone at T c = 122.6 K. *Cryst. Growth Des.* **2013**, *13*, 4571–4582. [CrossRef]
7. Sacchi, P.; Loconte, L.; Macetti, G.; Rizzato, S.; Lo Presti, L. Correlations of Crystal Structure and Solubility in Organic Salts: The Case of the Antiplasmodial Drug Piperaquine. *Cryst. Growth Des.* **2019**, *19*, 1399–1410. [CrossRef]
8. Nakamura, A.; Ishida, T.; Fushinobu, S.; Kusaka, K.; Tanaka, I.; Inaka, K.; Higuchi, Y.; Masaki, M.; Ohta, K.; Kaneko, S.; et al. Phase-diagram-guided method for growth of a large crystal of glycoside hydrolase family 45 inverting cellulase suitable for neutron structural analysis. *J. Synchrotron Radiat.* **2013**, *20*, 859–863. [CrossRef]
9. Haas, C.; Drenth, J. Understanding protein crystallization on the basis of the phase diagram. *J. Cryst. Growth* **1999**, *196*, 388–394. [CrossRef]
10. Govada, L.; Chayen, N. Choosing the Method of Crystallization to Obtain Optimal Results. *Crystals* **2019**, *9*, 106. [CrossRef]
11. Chayen, N. Methods for separating nucleation and growth in protein crystallisation. *Prog. Biophys. Mol. Biol.* **2005**, *88*, 329–337. [CrossRef] [PubMed]
12. Threlfall, T. Crystallisation of Polymorphs: Thermodynamic Insight into the Role of Solvent. *Org. Process Res. Dev.* **2000**, *4*, 384–390. [CrossRef]
13. Kee, N.C.S.; Tan, R.B.H.; Braatz, R.D. Semiautomated Identification of the Phase Diagram for Enantiotropic Crystallizations using ATR-FTIR Spectroscopy and Laser Backscattering. *Ind. Eng. Chem. Res.* **2011**, *50*, 1488–1495. [CrossRef]
14. Li, H.; Wang, K.; Sun, Y.; Lollar, C.T.; Li, J.; Zhou, H.-C. Recent advances in gas storage and separation using metal–organic frameworks. *Mater. Today* **2018**, *21*, 108–121. [CrossRef]
15. Dhakshinamoorthy, A.; Li, Z.; Garcia, H. Catalysis and photocatalysis by metal organic frameworks. *Chem. Soc. Rev.* **2018**, *47*, 8134–8172. [CrossRef]
16. Kreno, L.E.; Leong, K.; Farha, O.K.; Allendorf, M.; Van Duyne, R.P.; Hupp, J.T. Metal–Organic Framework Materials as Chemical Sensors. *Chem. Rev.* **2012**, *112*, 1105–1125. [CrossRef] [PubMed]
17. Keskin, S.; Kızılel, S. Biomedical Applications of Metal Organic Frameworks. *Ind. Eng. Chem. Res.* **2011**, *50*, 1799–1812. [CrossRef]
18. Northrop, B.H.; Zheng, Y.-R.; Chi, K.-W.; Stang, P.J. Self-Organization in Coordination-Driven Self-Assembly. *Acc. Chem. Res.* **2009**, *42*, 1554–1563. [CrossRef]
19. Chakrabarty, R.; Mukherjee, P.S.; Stang, P.J. Supramolecular Coordination: Self-Assembly of Finite Two- and Three-Dimensional Ensembles. *Chem. Rev.* **2011**, *111*, 6810–6918. [CrossRef]
20. Dey, C.; Kundu, T.; Biswal, B.P.; Mallick, A.; Banerjee, R. Crystalline metal-organic frameworks (MOFs): Synthesis, structure and function. *Acta Crystallogr. Sect. B Struct. Sci. Cryst. Eng. Mater.* **2014**, *70*, 3–10. [CrossRef]
21. Zhang, B.; Zhang, J.; Liu, C.; Sang, X.; Peng, L.; Ma, X.; Wu, T.; Han, B.; Yang, G. Solvent determines the formation and properties of metal–organic frameworks. *RSC Adv.* **2015**, *5*, 37691–37696. [CrossRef]
22. Moreno, A.; Rosales-Hoz, M.J. Crystal growth of inorganic, organic, and biological macromolecules in gels. *Prog. Cryst. Growth Charact. Mater.* **2017**, *63*, 63–71. [CrossRef]

23. Prieto, M.; Fernández-Diaz, L.; López-Andrés, L.; López-Andrés, S. Supersaturation evolution and first precipitate location in crystal growth in gels; application to barium and strontium carbonates. *J. Cryst. Growth* **1989**, *98*, 447–460. [CrossRef]

24. Garcia-Ruiz, J.M. The uses of crystal growth in gels and other diffusing-reacting systems. *Key Eng. Mater.* **1991**, *58*, 87–106. [CrossRef]

25. Rizzato, S.; Moret, M.; Merlini, M.; Albinati, A.; Beghi, F. Crystal growth in gelled solution: Applications to coordination polymers. *CrystEngComm* **2016**, *18*, 2455–2462. [CrossRef]

26. Carlucci, L.; Ciani, G.; Garcia-Ruiz, J.M.; Moret, M.; Proserpio, D.M.; Rizzato, S. Crystallization Behavior of Coordination Polymers. 1: Kinetic and Thermodynamic Features of 1,3-Bis(4-pyridyl)propane/MCl2 Systems. *Cryst. Growth Des.* **2009**, *9*, 5024–5034. [CrossRef]

27. Robert, M.-C.; Vidal, O.; Garcia-Ruiz, J.-M.; Otalora, F. *Crystallization in gels and related methods*; Oxford University Press: New York, NY, USA, 1999; pp. 149–175.

28. Luft, J.R.; Newman, J.; Snell, E.H. Crystallization screening: The influence of history on current practice. *Acta Crystallogr. Sect. F Struct. Biol. Commun.* **2014**, *70*, 835–853. [CrossRef]

29. Sinder, M.I. Crystallization in gels. In *Proceedings of the Fiz. Krist.*; Kalinin. Gos. Univ.: Moscow, Russia, 1984; pp. 112–113.

30. Carlucci, L.; Ciani, G.; Moret, M.; Proserpio, D.M.; Rizzato, S. Monitoring the Crystal Growth and Interconversion of New Coordination Networks in the Self-assembly of MCl2 Salts (M = Co, Ni, Cu, Cd) and 1,3-Bis(4-pyridyl)propane. *Chem. Mater.* **2002**, *14*, 12–16. [CrossRef]

31. Luo, F.; Che, Y.; Zheng, J. Synthesis, structure and characteristics of one 3D 2-fold interpenetrating net with rare 42638 topology. *Inorg. Chem. Commun.* **2006**, *9*, 856–858. [CrossRef]

32. Oaki, Y.; Imai, H. Experimental Demonstration for the Morphological Evolution of Crystals Grown in Gel Media. *Cryst. Growth Des.* **2003**, *3*, 711–716. [CrossRef]

33. Petrova, R.I.; Swift, J.A. Habit Changes of Sodium Bromate Crystals Grown from Gel Media. *Cryst. Growth Des.* **2002**, *2*, 573–578. [CrossRef]

34. Pauchet, M.; Morelli, T.; Coste, S.; Malandain, J.-J.; Coquerel, G. Crystallization of (±)-Modafinil in Gel: Access to Form I, Form III, and Twins. *Cryst. Growth Des.* **2006**, *6*, 1881–1889. [CrossRef]

35. Diao, Y.; Whaley, K.E.; Helgeson, M.E.; Woldeyes, M.A.; Doyle, P.S.; Myerson, A.S.; Hatton, T.A.; Trout, B.L. Gel-induced selective crystallization of polymorphs. *J. Am. Chem. Soc.* **2012**, *134*, 673–684. [CrossRef] [PubMed]

36. Estroff, L.A.; Hamilton, A.D. At the Interface of Organic and Inorganic Chemistry: Bioinspired Synthesis of Composite Materials. *Chem. Mater.* **2001**, *13*, 3227–3235. [CrossRef]

37. Rizzato, S.; Moret, M.; Beghi, F.; Lo Presti, L. Crystallization and structural properties of a family of isotopological 3D-networks: The case of a 4,4′-bipy ligand–M^{2+} triflate system. *CrystEngComm* **2018**, *20*, 3784–3795. [CrossRef]

38. Garcia-Ruiz, J.M.; Gavira, J.A.; Otalora, F.; Guasch, A.; Coll, M. Reinforced protein crystals. *Mater. Res. Bull.* **1998**, *33*, 1593–1598. [CrossRef]

39. Yang, T.; Han, Y. Quantitatively Relating Diffusion and Reaction for Shaping Particles. *Cryst. Growth Des.* **2016**, *16*, 2850–2859. [CrossRef]

40. Lagzi, I.; Ueyama, D. Pattern transition between periodic Liesegang pattern and crystal growth regime in reaction-diffusion systems. *Chem. Phys. Lett.* **2009**. [CrossRef]

41. Dirany, N.; Arab, M.; Moreau, A.; Valmalette, J.C.; Gavarri, J.R. Hierarchical design and control of NaCe(WO4)2 crystals: Structural and optical properties. *CrystEngComm* **2016**, *18*, 6579–6593. [CrossRef]

42. Srivastava, R.; Srivastava, P.K. Nanostructured diffusion-limited-aggregation crystal pattern formation in a reactive microemulsion system. *Adv. Nat. Sci. Nanosci. Nanotechnol.* **2014**, *5*, 015018. [CrossRef]

43. *Morphogenesis and Pattern Formation in Biological Systems*; Sekimura, T.; Noji, S.; Ueno, N.; Maini, P.K. (Eds.) Springer Japan: Tokyo, Japan, 2003; ISBN 978-4-431-65960-0.

44. Pina, C.M.; Fernández-Díaz, L.; Astilleros, J.M. Nucleation and Growth of Scheelite in a Diffusing-Reacting System. *Cryst. Res. Technol.* **2000**, *35*, 1015–1022. [CrossRef]

45. Prieto, M.; Fernández-Diaz, L.; López-Andrés, S. Spatial and evolutionary aspects of nucleation in diffusing-reacting systems. *J. Cryst. Growth* **1991**, *108*, 770–778. [CrossRef]

46. Desai, C.C.; Rai, J.L. Growth kinetics of tin iodide single crystals in silica gels. *Surf. Technol.* **1982**, *15*, 25–32. [CrossRef]

47. Cubillas, P.; Anderson, M.W. Synthesis Mechanism: Crystal Growth and Nucleation. In *Zeolites and Catalysis*; Wiley-VCH Verlag GmbH & Co. KGaA: Hoboken, NJ, USA, 2010; pp. 1–55. ISBN 9783527630295.

48. Raj, A.M.E.; Jayanthi, D.D.; Jothy, V.B.; Jayachandran, M.; Sanjeeviraja, C. Growth aspects of barium oxalate monohydrate single crystals in gel medium. *Cryst. Res. Technol.* **2008**, *43*, 1307–1313. [CrossRef]

49. Garcia-Ruiz, J.M.; Moreno, A. Growth kinetics of protein single crystals in the gel acupuncture technique. *J. Cryst. Growth* **1997**, *178*, 393–401. [CrossRef]

50. Pyankova, L.A.; Punin, Y.O.; Bocharov, S.N.; Shtukenberg, A.G. Growth kinetics and micromorphology of $NH_4Cl:Mn^{2+}$ crystals formed in the NH_4Cl-$MnCl_2$-H_2O-$CONH_3$ system. *Crystallogr. Rep.* **2012**, *57*, 317–326. [CrossRef]

51. Gao, P.; Gu, M.; Xiao, L.-L. Understanding the growth mechanism of CuI crystals during gel growth experiments. *Cryst. Res. Technol.* **2008**, *43*, 496–501. [CrossRef]

52. Al-Ghoul, M.; Issa, R.; Hmadeh, M. Synthesis, size and structural evolution of metal–organic framework-199 via a reaction–diffusion process at room temperature. *CrystEngComm* **2017**, *19*, 608–612. [CrossRef]

53. García-Ruiz, J.M.; Otálora, F.; Novella, M.L.; Gavira, J.A.; Sauter, C.; Vidal, O. A supersaturation wave of protein crystallization. *J. Cryst. Growth* **2001**, *232*, 149–155. [CrossRef]

54. Arend, H.; Perison, J. The gel growth of $Ag_2H_3IO_6$ crystals. *Mater. Res. Bull.* **1971**, *6*, 1205–1210. [CrossRef]